The Journal of Chemical Physics

Ion-atom-atom three-body recombination: From the cold to the thermal regime

Cite as: J. Chem. Phys. **158**, 024103 (2023); https://doi.org/10.1063/5.0134132
Submitted: 08 November 2022 • Accepted: 23 December 2022 • Accepted Manuscript Online: 26 December 2022 • Published Online: 09 January 2023

Marjan Mirahmadi and Jesús Pérez-Ríos

The Journal of Chemical Physics ARTICLE scitation.org/journal/jcp

Ion-atom-atom three-body recombination: From the cold to the thermal regime

Cite as: J. Chem. Phys. 158, 024103 (2023); doi: 10.1063/5.0134132
Submitted: 8 November 2022 • Accepted: 23 December 2022 •
Published Online: 9 January 2023

Marjan Mirahmadi[1,a] and Jesús Pérez-Ríos[2,b]

AFFILIATIONS

[1] Fritz-Haber-Institut der Max-Planck-Gesellschaft, Faradayweg 4-6, D-14195 Berlin, Germany
[2] Department of Physics and Astronomy, Stony Brook University, Stony Brook, New York 11794, USA and Institute for Advanced Computational Science, Stony Brook University, Stony Brook, New York 11794, USA

Note: This paper is part of the 2022 JCP Emerging Investigators Special Collection.
[a] **Electronic mail:** mirahmadi@fhi-berlin.mpg.de
[b] **Author to whom correspondence should be addressed:** jesus.perezrios@stonybrook.edu

ABSTRACT

We present a study on ion–atom–atom reaction $A + A + B^+$ in a wide range of systems and collision energies ranging from 100 μK to 10^5 K, analyzing two possible products: molecules and molecular ions. The dynamics is performed via a direct three-body formalism based on a classical trajectory method in hyperspherical coordinates developed in Pérez-Ríos *et al.* [J. Chem. Phys. **140**, 044307 (2014)]. Our chief finding is that the dissociation energy of the molecular ion product acts as a threshold energy, separating the low- and high-energy regimes. In the low-energy regime, the long-range tail of the three-body potential dictates the fate of the reaction and the main reaction product. On the contrary, in the high-energy regime, the short-range of atom–atom and atom–ion interaction potential dominate the dynamics, enhancing molecular formation.

I. INTRODUCTION

Three-body recombination, also known as ternary association, is a termolecular reaction, leading to the formation of a bound state between two of the colliding particles, i.e., $A + A + A \rightarrow A_2 + A$. Three-body recombination processes play a vital role in many areas of physics and chemistry, such as atomic and molecular processes in the ultracold regime,[1–12] chemical physics,[13–21] cold chemistry,[22,23] plasma physics,[24–26] astrophysics,[27–30] and atmospheric physics.[31–34]

In particular, ion–atom–atom, three-body recombination processes have received much attention—thanks to the recent developments in producing hybrid ion–atom systems. In the cold regime, this process (for high enough atomic densities) is the primary ion loss mechanism,[35–37] leading to newly formed charged products.[10,11] Furthermore, this few-body scenario gives insight into the problem of charged impurities in an ultracold atomic gas,[22,38] relevant to many-body physics. Ion–atom–atom three-body recombination reactions involving rare gases are of fundamental interest in radiation physics[39–42] or in the case of hydrogen and deuterium, in plasma physics.[24,25] In all the mentioned areas, except for plasma physics, the reaction occurs at temperatures $\lesssim$1 K. As a result, most theoretical efforts have been focused on the low collision energy regime. Therefore, a comprehensive and general study of ion–atom–atom three-body processes in a wide range of collision energies is still lacking.

Herein, we investigate the direct ion–atom–atom three-body reaction $A + A + B^+$, based on a classical trajectory method in hyperspherical coordinates. During this process, two different products might form: molecular ions, AB^+, and neutral molecules, A_2, from $A + A + B^+ \rightarrow A + AB^+$ and $A + A + B^+ \rightarrow A_2 + B^+$ reactions, respectively. We aim to study both reaction products by comparing their formation rates based on the strengths of the long-range two-body interactions—$-C_6/r^6$ (atom–atom) and $-C_4/r^4$ (ion–atom).

To this end, we introduce an effective (hyper-) radial potential in hyperspherical coordinates and find the power-dependence of this potential over a wide range of C_6 and C_4 values. Using this potential, we are able to confirm the previously derived threshold law for ion–neutral–neutral three-body recombination[10,43] at low temperatures and establish the range for its validity. Moreover, we find new and intriguing scenarios in which the branching ratio of the product

states after three-body recombination deviates from the expected threshold law in the cold regime.

This paper is organized as follows: In Sec. II, we introduce the Hamiltonian and explain the method. In Sec. III, an effective long-range radial potential has been derived to characterize the three-body collision based on its power-dependence. Using these findings, a classical threshold law is established in Sec. IV. In Sec. V, we investigate the formation probabilities and recombination rates for different products through several examples of three-body reactions. Finally, Sec. VI provides a summary and outlines the prospects for future applications of the present work.

II. A CLASSICAL TRAJECTORY METHOD IN HYPERSPHERICAL COORDINATES

The dynamics of a system consisting of three particles with masses m_i $(i = 1, 2, 3)$, interacting via the potential $V(\vec{r}_1, \vec{r}_2, \vec{r}_3)$ is governed by the Hamiltonian

$$H = \frac{\vec{p}_1^{\,2}}{2m_1} + \frac{\vec{p}_2^{\,2}}{2m_2} + \frac{\vec{p}_3^{\,2}}{2m_3} + V(\vec{r}_1, \vec{r}_2, \vec{r}_3), \tag{1}$$

with $\vec{r}_i$ and $\vec{p}_i$ being the position and momentum vectors of the i-th particle, respectively. Throughout the present work, we use the pairwise additive approximation, which states that the total potential of an N-body system is the sum of all two-body interactions in the system. In particular, we introduce the pairwise potentials $U(r_{ij})$ for neutral–neutral interactions and $\tilde{U}(r_{ij})$ for charged–neutral interactions. As a result, the interaction potential in Eq. (1) read as

$$V(\vec{r}_1, \vec{r}_2, \vec{r}_3) = U(r_{12}) + \tilde{U}(r_{23}) + \tilde{U}(r_{31}), \tag{2}$$

where $r_{ij} = |\vec{r}_j - \vec{r}_i|$.

It is convenient to study the three-body problem in Jacobi coordinates[44,45] related to the position vectors in Cartesian coordinates by the relations

$$\begin{aligned} \vec{\rho}_1 &= \vec{r}_2 - \vec{r}_1, \\ \vec{\rho}_2 &= \vec{r}_3 - \vec{R}_{CM12}, \\ \vec{\rho}_{CM} &= \frac{m_1\vec{r}_1 + m_2\vec{r}_2 + m_3\vec{r}_3}{M}, \end{aligned} \tag{3}$$

where $M = m_1 + m_2 + m_3$ is the total mass, and $\vec{R}_{CM12} = (m_1\vec{r}_1 + m_2\vec{r}_2)/(m_1 + m_2)$ and $\vec{\rho}_{CM}$ are the center-of-mass vectors of the two-body and three-body systems, respectively. The Jacobi vectors are illustrated as the green vectors in Fig. 1. Due to the conservation of the total linear momentum ($\vec{\rho}_{CM}$ is a cyclic coordinate), we can omit the degrees of freedom of the center of mass. Thus, the Hamiltonian (1) will be transformed to

$$H = \frac{\vec{P}_1^2}{2\mu_{12}} + \frac{\vec{P}_2^2}{2\mu_{3,12}} + V(\vec{\rho}_1, \vec{\rho}_2), \tag{4}$$

with reduced masses $\mu_{12} = m_1m_2/(m_1 + m_2)$ and $\mu_{3,12} = m_3(m_1 + m_2)/M$. $\vec{P}_1$ and $\vec{P}_2$ indicate the conjugated momenta of the Jacobi vectors $\vec{\rho}_1$ and $\vec{\rho}_2$, respectively. It is worth mentioning that the relations given by Eq. (3) indicate a canonical transformation, and, consequently, Hamilton's equations of motion are invariant under the transformation to Jacobi coordinates.

A. Scattering problem in hyperspherical coordinates

It is well-known that an N-body collision in a three-dimensional (3D) space can be mapped onto a scattering problem of a single particle with a definite momentum moving toward a scattering center in an $(N-3)$-dimensional space. In particular, the independent relative coordinates of the three-body system, associated with the Hamiltonian (4) in the 3D space, are mapped onto the degrees of freedom of a single particle moving toward a scattering center in a six-dimensional (6D) space. We choose a 6D space parameterized by hyperspherical coordinates consisting of a hyper-radius R, and five hyperangles α_j (with $j = 1, 2, 3, 4, 5$), where $0 \le \alpha_1 < 2\pi$ and $0 \le \alpha_{j>1} \le \pi$.[46–48]

The volume element in this coordinate system is given by

$$\begin{aligned} d\tau &= R^5 dR d\Omega, \\ &= R^5 dR \prod_{j=1}^{5} \sin^{j-1}(\alpha_j) d\alpha_j. \end{aligned} \tag{5}$$

The position and momentum vectors in this space can be constructed from the Jacobi vectors and their conjugated momenta as[23,48]

$$\vec{\rho} = \begin{pmatrix} \vec{\rho}_1 \\ \vec{\rho}_2 \end{pmatrix} \tag{6}$$

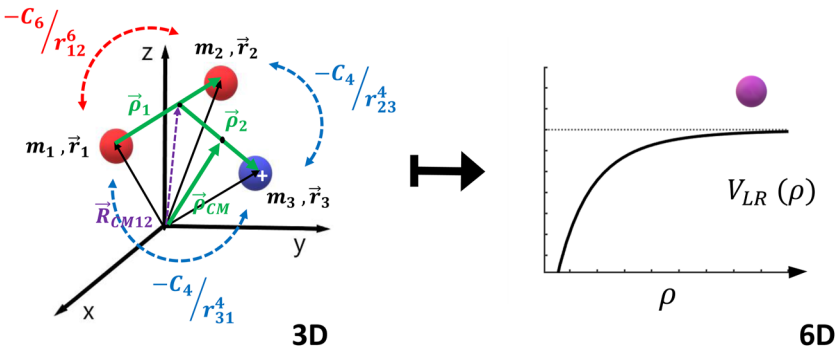

FIG. 1. A schematic illustration of the long-range two-body interactions between three particles in 3D space and their counterpart, $V_{LR}(\rho)$, for a single particle in the 6D space. Jacobi coordinates for the three-body problem are shown as green vectors. Black arrows indicate the position of the three particles in Cartesian coordinates, and the purple arrow indicates the two-body center-of-mass vector $\vec{R}_{CM12}$.

and

$$\vec{P} = \begin{pmatrix} \sqrt{\frac{\mu}{\mu_{12}}}\vec{P}_1 \\ \sqrt{\frac{\mu}{\mu_{3,12}}}\vec{P}_2 \end{pmatrix}, \tag{7}$$

respectively. Here, $\mu = \sqrt{m_1 m_2 m_3/M}$ is the three-body reduced mass. By using Eqs. (6) and (7), the Hamiltonian in the 6D space reads as

$$H^{6D} = \frac{\vec{P}^2}{2\mu} + V(\vec{\rho}). \tag{8}$$

The concept of classical cross section σ for the scattering problem in the 3D space can be extended to the 6D space by visualizing it as an area in a five-dimensional hyperplane (embedded in the 6D space) perpendicular to the initial (6D) momentum vector $\vec{P}_0$. Thus, the impact parameter vector $\vec{b}$ in the 6D space can be defined as the projection of the initial position vector $\vec{\rho}_0$ on this hyperplane. Therefore, the necessary condition $\vec{b}\cdot\vec{P}_0 = 0$ is satisfied.

Note that by treating three-body collisions as a scattering problem of a single particle in a 6D space, we can uniquely define the initial conditions and the impact parameter as single entities (in the 6D space). Therefore, it is possible to characterize the outcome of a three-body process as a function of the impact parameter $\vec{b}$ and the initial momentum $\vec{P}_0$. In particular, for three-body recombination, the total cross section is given by[23,48]

$$\sigma_{\rm rec}(E_c) = \frac{\int \mathcal{P}(\vec{P}_0,\vec{b}) b^4\, db\, d\Omega_b d\Omega_{P_0}}{\int d\Omega_{P_0}} = \frac{8\pi^2}{3}\int_0^{b_{\rm max}(E_c)} \mathcal{P}(E_c,b) b^4 db, \tag{9}$$

after averaging over different orientations of $\vec{P}_0$. In Eq. (9), $d\Omega_b$ and $d\Omega_{P_0}$ denote the differential elements of the solid hyperangle associated with vectors $\vec{b}$ and $\vec{P}_0$, respectively, where $\Omega_b = 8\pi^2/3$. The so-called opacity function $\mathcal{P}$ in Eq. (9) is the probability of a recombination event as a function of the impact parameter b and collision energy E_c [obtained from $E_c = P_0^2/(2\mu)$]. The angular dependence of the opacity function $\mathcal{P}(\vec{P}_0,\vec{b})$, which depends on both, the direction and magnitude of the impact parameter and initial momentum vectors, has been averaged out by means of the Monte Carlo method explained further below. $b_{\rm max}$ represents the largest impact parameter for which three-body recombination occurs, or in other words, $\mathcal{P}(E_c,b) = 0$ for $b > b_{\rm max}$. Consequently, the energy-dependent three-body recombination rate is given by

$$k_3(E_c) = \sqrt{\frac{2E_c}{\mu}}\sigma_{\rm rec}(E_c). \tag{10}$$

B. Computational details

The initial orientation of vectors $\vec{P}_0$ and $\vec{b}$ in the 6D space are sampled randomly from probability distribution functions associated with the appropriate angular elements in hyperspherical coordinates (see Ref. 23). For the sake of simplicity and without loss of generality, we choose the z axis in 3D space to be parallel to the Jacobi momentum vector $\vec{P}_2$. Note that the condition $\vec{b}\cdot\vec{P}_0 = 0$ is also implemented in the calculations.

The opacity function $\mathcal{P}(E_c,b)$ for a given collision energy E_c and magnitude of impact parameter b is achieved by dividing the number of classical trajectories that lead to the recombination events, n_r, by the total number of trajectories simulated, n_t.[48] Thus,

$$\mathcal{P}(E_c,b) \approx \frac{n_r(E_c,b)}{n_t(E_c,b)} \pm \frac{\sqrt{n_r(E_c,b)}}{n_t(E_c,b)}\sqrt{\frac{n_t(E_c,b)-n_r(E_c,b)}{n_t(E_c,b)}}, \tag{11}$$

where the second term in Eq. (11) is the statistical error, owing to the inherently stochastic nature of the Monte Carlo technique. For the results reported in this work, for each initial pair of (E_c,b), the number of total trajectories varies between $n_t = 3\times10^3$ and $n_t = 10^5$ to keep the relative error in calculated $k_3(E_c)$ rate coefficients below 5%.

For the results presented here, Hamilton's equations have been solved using the "ode113" of Matlab ordinary differential equation (ODE) suite. This is a variable-step/variable-order predictor–corrector (PECE of orders 1–13) implementation of the Adams–Bashforth–Moulton methods.[49] The acceptable error for each time-step has been determined by absolute and relative tolerances equal to 10^{-15} and 10^{-13}, respectively. The total energy is conserved during collisions to at least four significant digits, and the magnitude of the total angular momentum vector, $J = |\vec{\rho}_1\times\vec{P}_1 + \vec{\rho}_2\times\vec{P}_2|$, is conserved to at least six significant digits. The initial magnitude of hyper-radius, $|\vec{\rho}_0|$, is generated randomly from the interval $[R_0-\delta R, R_0+\delta R]\,a_0$ centered around a suitable R_0, which fulfills the condition for three particles to be initially in a uniform rectilinear state of motion. Here, a_0 is the Bohr radius ($\approx 5.29\times10^{-11}$m).

III. LONG-RANGE (HYPER-) RADIAL POTENTIAL

It is possible to characterize the A + A + B^+ three-body recombination reaction and its products at low temperatures based on the long-range behavior of the two-body potentials, i.e., $U(r_{12}) \to -C_6/r_{12}^6$ for A_2 and $\tilde{U}(r_{23}) \to -C_4/r_{23}^4$ and $\tilde{U}(r_{31}) \to -C_4/r_{31}^4$ for AB^+. To this end, we find the corresponding long-range potential in the 6D space relevant for the classical trajectory method explained in Sec. II. Hence, the effective long-range potential in hyperspherical coordinates can be obtained from the following relation (see Fig. 1):

$$V_{LR}(\vec{\rho}) = -\frac{C_6}{r_{12}^6} - \frac{C_4}{r_{23}^4} - \frac{C_4}{r_{31}^4}, \tag{12}$$

where $C_6 = C_6^{A_2}$ is the van der Waals dispersion coefficient, and $C_4 = C_4^{AB^+}$ is half of the atom (A) polarizability (in a.u.).

Noting Eqs. (3) and (6), potential $V_{LR}(\vec{\rho})$ depends on the magnitude of the 6D position vector, $\rho = |\vec{\rho}|$, as well as the hyperangles $(\alpha_1,\alpha_2,\alpha_3,\alpha_4,\alpha_5)$associated with it. Thus, to find the radial dependence of this potential, labeled $V_{LR}(\rho)$ in the schematic illustration in Fig. 1, we solve Eq. (12) for randomly sampled hyperangles with appropriate weights [given in Eq. (5)], ensuring a uniform sampling of the configuration space (for more details see Refs. 21 and 50). Considering C_4 and C_6 constants, the (hyper-) radial potential reads as

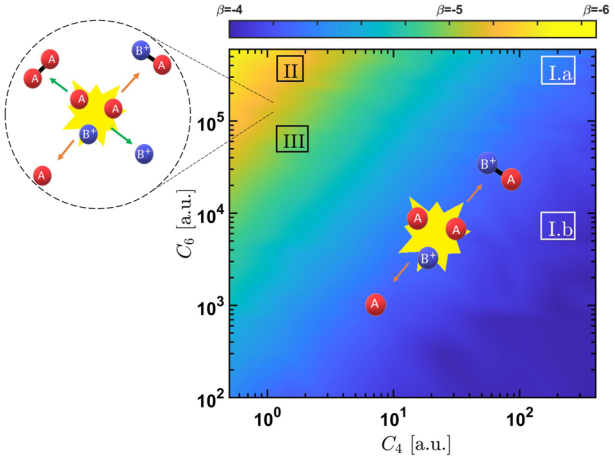

FIG. 2. Heat map of visualizing the parameter β as a function of long-range two-body interaction coefficients C_4 and C_6 in the log–log scale. Letters indicate the examples chosen from different regimes ($\beta = -4, -5$, and -6). The schematic illustrations display the dominant reactions at low collision energies.

$$V_{LR}(\rho) = -C_{\text{eff}}\rho^{\beta}. \tag{13}$$

Consequently, the power β can be considered as a function $\beta(C_6, C_4)$.

Figure 2 displays the parameter β as a function of $C_6 \in [10^2, 6 \times 10^5]$ and $C_4 \in [0.5, 400]$, in a.u. In this figure, we identify three main regimes associated with $\beta \approx -6$ (yellow color), $\beta \approx -4$ (blue color), and an intermediate regime $\beta \approx -5$ (greenish yellow color). Different values of β translate into the preponderance of a given reaction product, as shown below. In particular, $\beta \approx -4$ represents a typical scenario in which the charged–neutral interaction dominates the course of the reaction, leading mainly to the formation of ions, as sketched in Fig. 2. On the contrary, $\beta \approx -6$ means that the neutral–neutral interaction is the most significant interaction, which translates into a larger production of neutral molecules.

Surprisingly enough, there is a last scenario in which both–neutral–neutral and neutral-charged interactions–have a considerable contribution, leading to $\beta \approx -5$. In such a case, the three-body recombination should lead to a similar amount of neutral molecules to molecular ions. However, this is an unexpected scenario, since the long-range two-body potentials are proportional to r_{ij}^{-4} and r_{ij}^{-6} for charged–neutral and neutral–neutral interactions, respectively, but the hyper-radial potential has the power-dependence ρ^{-5}.

It is worth mentioning that the coefficients C_6 and C_4 in most ion–atom–atom reactions are associated with $\beta \approx -4$.

IV. GENERALIZED CLASSICAL THRESHOLD LAW

The general trend of the three-body recombination rate as a function of the collision energy (E_c) fulfills a threshold law in the low-energy regime. In particular, considering the fact that the long-range tail of the potential dominates the recombination rate at low energies, we can derive a classical threshold law associated with the quantum s-wave scattering, i.e., zero quantum angular momentum. In classical scattering, one may define the maximum impact parameter, $b_{\max}$, as the distance at which the collision energy is comparable to the strength of the interaction potential, i.e., $E_c = C_6 r_{12}^{-6} + C_4 r_{23}^{-4} + C_4 r_{31}^{-4}$ in 3D space, or equivalently, $E_c = C_{\text{eff}}\rho^{\beta}$, in 6D space. Note that the coefficient C_{eff} can be obtained for different values of β (for more details, see Ref. 21); however, here, we are only interested in the power-law dependence of the $k_3(E_c)$. Therefore, we derive the following relation for $b_{\max}$,

$$b_{\max} \propto E_c^{1/\beta}. \tag{14}$$

The geometric cross section is obtained by setting $\mathcal{P}(E_c, b) = 1$ for $b \le b_{\max}$ (also known as the rigid-sphere model) in Eq. (9). Thus, upon substituting Eq. (14) into Eq. (9), we find the energy-dependence of the geometric cross section as

$$\sigma_{\text{rec}}(E_c) = \frac{8\pi^2}{3}\int_0^{b_{\max}(E_c)} b^4 db \propto E_c^{5/\beta}. \tag{15}$$

Employing Eq. (10), the three-body recombination rate can be calculated as a function of collision energy as

$$k_3(E_c) \propto E_c^{(10+\beta)/(2\beta)}. \tag{16}$$

Setting $\beta = -4$, Eqs. (15) and (16) lead to $\sigma_{\text{rec}}(E_c) \propto E_c^{-5/4}$ and $k_3(E_c) \propto E_c^{-3/4}$. This result verifies the threshold law given in Refs. 10 and 43, which has been obtained under the assumption that only ion–atom interaction dictates the outcome of the three-body recombination. This is in accordance with our findings displayed in Fig. 2 and the related discussion in Sec. III. Note that the rate given by Eq. (16) accounts for both A_2 and AB^+ products of the three-body recombination. However, as is discussed below, in this scenario, AB^+ molecules are the main reaction product. In the two other regimes, i.e., $\beta = -5$ and -6, the power-law yields $k_3(E_c) = E_c^{-1/3}$ and $k_3(E_c) = E_c^{-1/2}$, respectively.

V. RESULTS AND DISCUSSION

The three-body recombination process $A + A + B^+$ might result in one of two different products, namely, the molecular ion, AB^+, and the neutral molecule, A_2. Molecular ions form through the reaction $A + A + B^+ \to A + AB^+$, whereas neutral molecule formation follows $A + A + B^+ \to A_2 + B^+$. In this section, we investigate each reaction's importance by using the opacity function, i.e., the probability of formation of each product as a function of the collision energy, E_c, and the impact parameter, b.

A. Low-energy regime

We consider three different scenarios related to the strengths of the long-range A_2 ($-C_6/r^6$) and AB^+ ($-C_4/r^4$) interactions, characterized by the parameter β introduced in Sec. III. Note that this characterization is only valid for the low-energy regime, at which the long-range interactions dictate the outcome of the three-body recombination reaction. In general, this region is assumed to correspond to the cold regime, i.e., $E_c \lesssim 1$ K.

Here, we calculate the opacity functions for four different scenarios labeled in Fig. 2: two examples, I.a and I.b, from the regime where the charged–neutral interaction is dominant ($\beta \approx -4$); the example II, for $\beta \approx -6$, where the neutral–neutral interaction is

TABLE I. Long-range coefficients of the pairwise potentials for four different regions highlighted in Fig. 2 for three-body recombination reactions, A + A + B^+. The values are given in a.u.

β	Label	C_6	C_4
−4	I.a	6×10^5	200
	I.b	6640	200
−6	II	7×10^4	1.85
−5	III	6×10^5	1.85

stronger; and example III for the intermediate region, i.e., $\beta \approx -5$. The corresponding C_6 and C_4 parameters are listed in Table I and the results are shown in Figs. 3–5. The relative error due to one standard deviation error, as is customary in Monte Carlo simulations [see Eq. (11)], for the lowest impact parameter $b = 0$ is ≈1%, and for the maximum impact parameter, b_{max}, it is ≈5%.

Note that in these calculations, the two-body potentials are of the form $U(r) = -C_6/r^6 + C_{12}/r^{12}$ for the atom–atom (A–A) interaction, whereas $\tilde{U}(r) = -C_4/r^4 + C_8/r^8$ for the ion–atom one ($A–B^+$).

1. Case I: Charged-neutral-dominated processes

Figure 3 shows the opacity functions of both products for two collision energies: 1 mK (left panel) and 10 K (right panel), for the I.a and I.b cases described above. The figure shows that although both

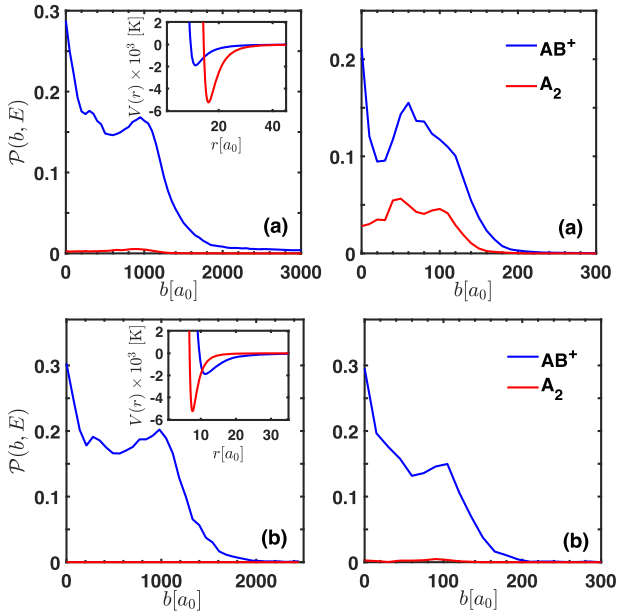

FIG. 3. The opacity function of each reaction product for $\beta \approx -4$ at collision energies E_c = 1 mK (left panels) and E_c = 10 K (right panels). The mass of the atom is the same as that of ^{133}Cs, and that of the ion corresponds to $^{87}Rb^+$. Pairwise potentials are shown in the inset. Here, $a_0 \approx 5.29 \times 10^{-11}$ m is the Bohr radius. Panel (a) corresponds to case I.a in Fig. 2, whereas panel (b) refers to the case I.b in Fig. 2.

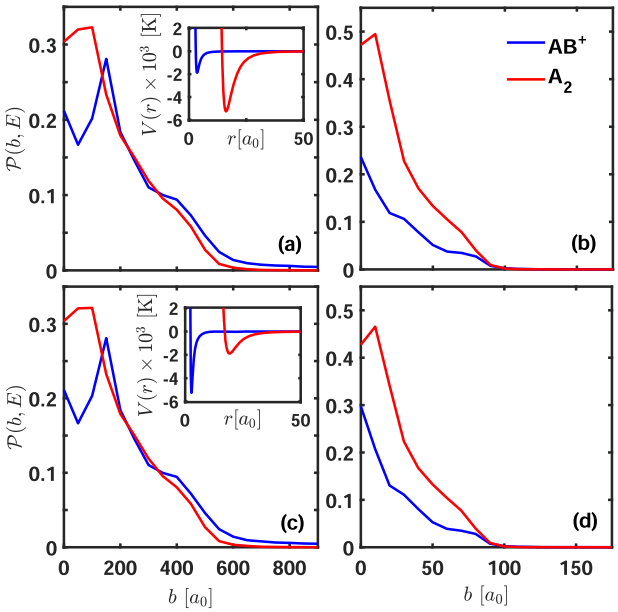

FIG. 4. The opacity function of each product for $\beta \approx -6$ (case II in Fig. 2) and collision energies E_c = 1 mK [panels (a) and (c)] and E_c = 10 K [panels (b) and (d)]. The mass of the atom is the same as that of ^{133}Cs, and for the ion, it corresponds to $^{87}Rb^+$. Plots in each row are calculated for different cases by changing the short-range properties of the pairwise potentials shown in the inset.

systems show a significant difference in the neutral–neutral interaction (the C_6 in I.a is ~100 times larger than that in I.b), AB^+ is the main product, regardless of the collision energy. At E_c = 1 mK, the opacity function for molecular ions (blue curve) is the same for the two cases under consideration. However, at E_c = 10 K, the opacity function changes case to case. For instance, at $b = 0$ and 10 K, the formation of molecular ions for the I.a case is 33% more probable than that in the I.b case. The same trend, although more abrupt, is observed for the opacity associated with molecule formation. In particular, at E_c = 10 K, I.a shows a somewhat substantial probability of formation of A_2 than I.b (where $\mathcal{P}$ of A_2 is ≈0) due to a larger C_6 value.

The opacity functions for the same long-range coefficients as in examples I.a and I.b, but with different short-range interaction potentials, have been calculated, and similar results have been obtained. This confirms that the short-range region of the pairwise interaction potential does not play a role in the three-body recombination rate at the low-energy regime.

2. Case II: Neutral-neutral-dominated processes

As can be seen in Fig. 4, when $\beta = -6$ (case II in Fig. 2), there is a boost in the formation of neutral molecules, regardless of the collision energy. At E_c = 1 mK [panels (a) and (c)], A_2 and AB^+ are formed with nearly the same probability. Indeed, for small impact parameters, the production of neural molecules exceeds that of molecular ions. The ratio between the formation of neutral molecules and molecular ions increases at E_c = 10 K [panels (b) and (d)]. Therefore, a system within the $\beta = -6$ regime will show a larger molecular formation rate than that in the case of $\beta = -4$.

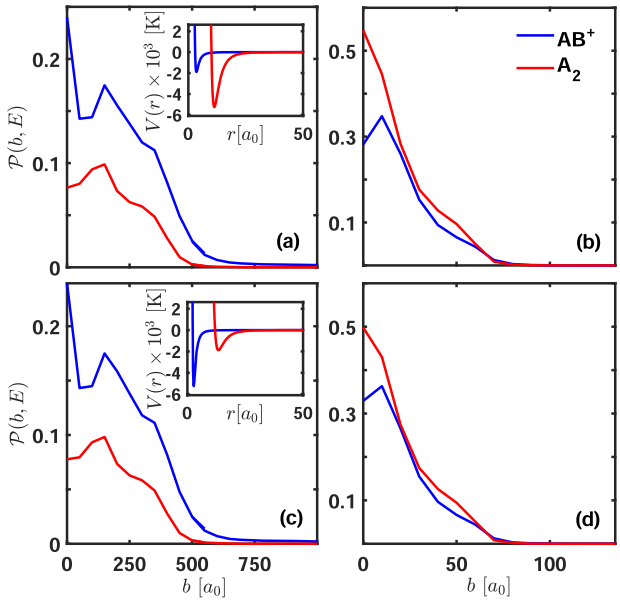

FIG. 5. The opacity function of each product for $\beta \approx -5$ (case III in Fig. 2) and collision energies E_c = 1 mK [panels (a) and (c)] and E_c = 10 K [panels (b) and (d)]. The mass of the atom is the same as that of ^{133}Cs, and for the ion, it corresponds to ^{87}Rb$^+$. Plots in each row are calculated for different cases by changing the short-range properties of the pairwise potentials shown in the inset.

Figures 4(c) and 4(d) display the opacity functions calculated for potentials with the same long-range tail as those in panels (a) and (b), but for different short-range properties of the potentials. As expected, for each collision energy, the opacities remain unchanged, independent of the nature of the short-range neutral–neutral or charged–neutral interactions. In other words, the short-range of the potential does not affect the three-body recombination reaction rate at low collision energies. This is similar to the conclusion for charged–neutral dominated processes (see Sec. V A 1). Moreover, note that in this region ($\beta \approx -6$), unlike the case of charged–neutral dominated processes ($\beta \approx -4$), the A + A + B$^+$ → A$_2$ + B$^+$ reaction process is not negligible. However, our results do not identify this process as the primary reaction, and molecular ion formation is still prominent.

3. Case III: The intermediate region

The opacity functions related to the intermediate region, $\beta = -5$, for two different collision energies, are displayed in Fig. 5. For E_c = 1 mK [panels (a) and (c)], we see that, even though the dominant product is AB$^+$, there is considerable probability for formation of A$_2$. For E_c = 10 K, the formation probabilities of neutral molecules and molecular ions are very close, except for small impact parameters ($b < 20$ a$_0$), where three-body recombination is prone to molecular formation in lieu of molecular ion formation.

Comparing Figs. 3–5, one can conclude that for systems with $\beta = -4$, the three-body recombination leads primarily to the formation of molecular ions, with negligible probability of the formation of neutral molecules. On the contrary, for systems with $\beta \approx -6$ or $\beta \approx -5$, molecular and molecular ion formation probabilities are comparable, and under certain conditions, the three-body recombination favors neutral molecule formation over molecular ions. A summary of our findings regarding the importance of different reactions in the low-energy regime has been illustrated schematically in Fig. 2 for the three different regions discussed above.

B. High-energy regime

In this section, we investigate three-body recombination processes at collision energies higher than previously considered. For these high energies, as will be shown, the short-range region of the pairwise interaction plays a pivotal role in the reaction dynamics. Therefore, categorizing collisions based on the long-range tail of the potentials is no longer valid.

We calculate the opacity function for two systems at two different collision energies (E_c = 3000 and 7000 K). In particular, the long-range tail of the charged–neutral and neutral–neutral potentials correspond to cases I.a and I.b in Fig. 2. The charged–neutral short-range potential is the same, whereas the neutral–neutral short-range potential varies. The results are shown in Fig. 6, where a more significant proportion of neutral molecules appear for the whole range of impact parameters, compared to those of Fig. 3. However, in virtue of the classical threshold law, three-body recombination should mostly lead to the formation of molecular ions, since $\beta \approx -4$. Therefore, the short range of the pairwise potential must play a major role for E_c = 3000 and 7000 K. In other words, the

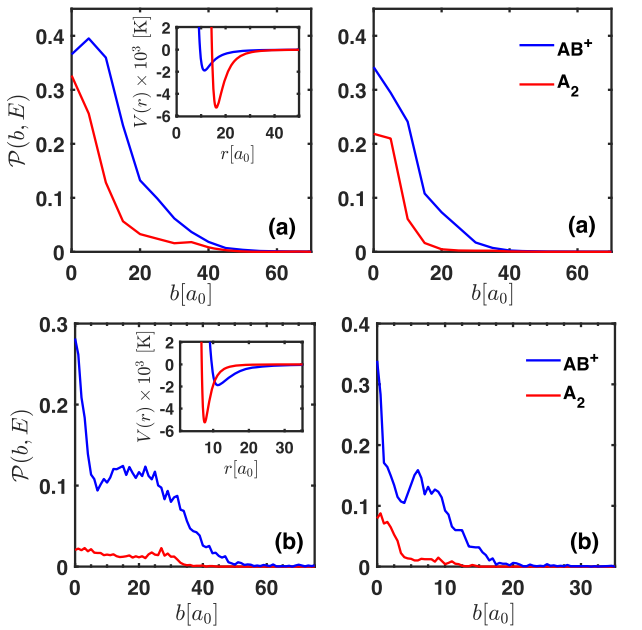

FIG. 6. The opacity function of each reaction product for $\beta \approx -4$ at collision energies E_c = 3000 K (left panels) and E_c = 7000 K (right panels). The mass of the atom is the same as that of ^{133}Cs, and for the ion, it corresponds to ^{87}Rb$^+$. Pairwise potentials are shown in the inset. Here, $a_0 \approx 5.29 \times 10^{-11}$ m is the Bohr radius. Panel (a) corresponds to case I.a in Fig. 2, whereas panel (b) refers to case I.b in Fig. 2.

systems under consideration enter into a new regime at high collision energies, dominated by short-range physics.

To characterize the transition from low-energy to high-energy regimes, it is necessary to study the formation of the two products—A_2 and AB^+—over a wide range of collision energies E_c, which is the goal of Sec. V C.

C. Study of representative systems

In this section, we focus on four ion–atom–atom systems. Three of them are representative of cold chemistry experiments in hybrid ion–atom traps, whereas the fourth is an important scenario for ion-mobility experiments. The energy-dependent three-body recombination rates are calculated via the classical trajectory method introduced in Sec. II over a wide range of collision energies between 10^{-4} and 10^5 K.

The first system under consideration is Cs + Cs + Sr^+, in which we assume that the Cs_2 and $CsSr^+$ are characterized by $X^1\Sigma_g^+$ and $A^1\Sigma^+$ potentials, respectively, with parameters given in Table II. The obtained three-body recombination rates for $CsSr^+$ (indicated by blue color) and Cs_2 (red color) molecules are shown in Fig. 7. In this figure, looking into the $CsSr^+$ rate coefficients, we identify two regimes associated with two different power-law behaviors (linear in the log–log scale). These two regimes meet at E_c equal to the dissociation energy of the $CsSr^+$ potential $D_e \approx 1888$ K (≈1312 cm^{-1}). Similarly, the two energy regimes can be recognized through the three-body recombination rates of Cs_2. However, in this case, the power-law dependence is different compared to molecular ion formation. In particular, the trend of $k_3(E_c)$ for the formation of neutral molecules changes twice—one slight change near the dissociation energy of $CsSr^+$ and a pronounced change at E_c comparable to the dissociation energy of Cs_2, i.e., $D_e \approx 5250$ K (≈3650 cm^{-1}).

At low collision energies, it is noticed, in Fig. 7, that the three-body recombination rate into Cs_2 is almost four orders of magnitude smaller than that into $CsSr^+$. Therefore, the dominant product is the molecular ion, and the formation rate of the neutral molecules is negligible; thus, the power-law derived in Sec. IV from Eq. (16) very well describes the trend of $k_3(E_c)$ for $CsSr^+$ formation (see the black dashed line). However, as energy increases, the ratio

TABLE II. Pairwise potential parameters used to calculate the reaction rates in different ion–atom–atom systems. The values are given in a.u.

System	State	Long-range	Short-range
Cs_2	$X^1\Sigma_g^{+a}$	$C_6 \approx 6.64 \times 10^3$	$C_{12} \approx 6.63 \times 10^8$
$CsSr^+$	$A^1\Sigma^{+b}$	$C_4 \approx 200$	$C_8 \approx 1.67 \times 10^6$
Rb_2	$X^1\Sigma_g^{+c}$	$C_6 \approx 4.71 \times 10^3$	$C_{12} \approx 3.05 \times 10^8$
$RbSr^+$	$A^1\Sigma^{+d}$	$C_4 \approx 160$	$C_8 \approx 1.46 \times 10^6$
$RbYb^+$	$A^1\Sigma^{+d}$	$C_4 \approx 160$	$C_8 \approx 1.68 \times 10^6$
He_2	$X^1\Sigma_g^{+e}$	$C_6 \approx 1.35$	$C_{12} \approx 1.38 \times 10^4$
He_2^+	$^2\Sigma_u^{+f}$	$C_4 \approx 0.69$	$C_8 \approx 1.32$

[a]Parameters are taken from Ref. 51.
[b]Parameters are taken from Refs. 52 and 53.
[c]Parameters are taken from Ref. 54.
[d]Parameters are taken from Refs. 52, 53, and 55.
[e]Parameters are taken from Ref. 56.
[f]Parameters are taken from Refs. 53, 57, and 58.

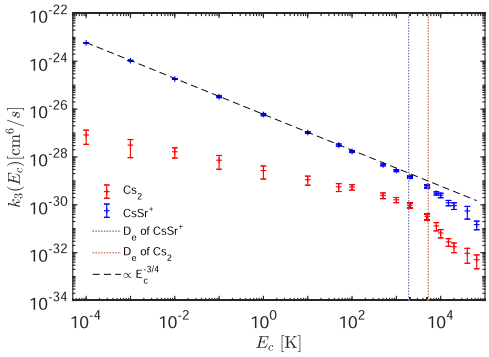

FIG. 7. Three-body recombination rates $k_3(E_c)$ for the Cs + Cs + Sr^+ reaction. Error bars are associated with the error in Eq. (11). The black dashed line indicates the power-law given in Eq. (16). The blue and red vertical dashed lines indicate the dissociation energies of $CsSr^+$ and Cs_2, respectively.

between both products decreases, eventually approaching the dissociation energy of the molecular ion. At this stage, the formation of Cs_2 cannot be neglected anymore, leading to a deviation from the derived power-law behavior via Eq. (16) ($\propto E_c^{-3/4}$), for E_c beyond the low-energy regime. In the high-energy regime, we observe that the three-body recombination rate into neutral molecules shows a steeper dependence on the collision energy compared to that into the molecular ions. This behavior is due to the difference in the short-range of the atom-ion potential $\propto r^{-8}$ and the atom–atom potential $\propto r^{-12}$, as explained in Ref. 20, for the formation of van der Waals molecules.

Next, we investigate the role of the short-range potential on the three-body recombination rate. In particular, we chose two systems with the same C_6 and C_4: Rb + Rb + Sr^+ and Rb + Rb + Yb^+. These systems share the same Rb_2 $X^1\Sigma_g^+$ potential, with parameters given in Table II. The ion–atom potentials are taken as $A^1\Sigma^+$, with the potential parameters listed in the same table. The results are shown in Figs. 8(a) and 8(b). These figures confirm the two regimes seen previously in Fig. 7, supporting the idea that the dissociation energy of the molecular ion is the threshold energy separating the low- from the high-energy regime.

Comparing the rates illustrated in Figs. 8(a) and 8(b), we notice that the power-law behavior of molecular ion's recombination rates (in blue) in the high-energy limit ($E_c > D_e$) depends on the short-range properties of the two-body potentials. In contrast, the three-body recombination rates $k_3(E_c)$ in the low-energy regime ($E_c < D_e$) obey the same power-law, which confirms that low energy collisions are dominated by the long-range tail of the ion–atom potential. Note that the dissociation energy of $RbSr^+$ is $D_e \approx 1380$ K (≈960 cm^{-1}) and that of $RbYb^+$ is $D_e \approx 1203$ K (≈836 cm^{-1}). Therefore, the ratio of the products in the low energy regime is almost independent of the short-range region of the atom–atom and ion–atom two-body potentials. On the other hand, similarly to Cs + Cs + Sr^+ collisions, in the high-energy regime, the formation rate of neutral molecules becomes more pronounced and competes with the formation rate of AB^+.

To confirm the generality of the discussion above, we consider the He + He + He^+ three-body recombination reaction, which is

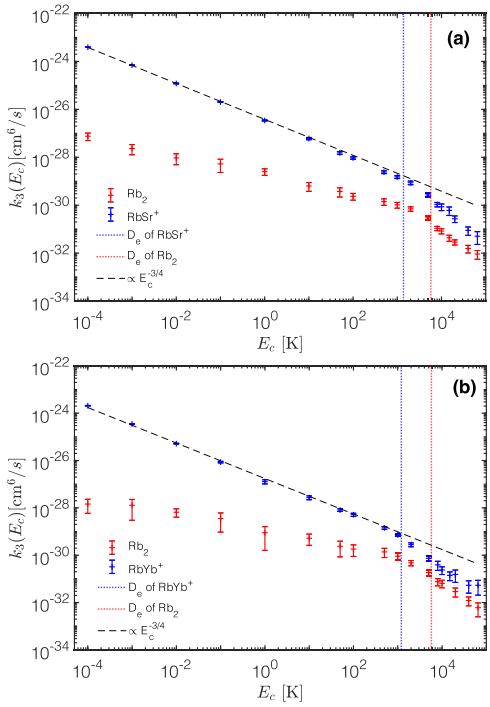

FIG. 8. Ion–atom–atomthree-body recombination. Panel (a) shows Rb + Rb + Sr^+ collisions, where the blue and red vertical dashed lines indicate the dissociation energies of $RbSr^+$ and Rb_2, respectively. Panel (b) stands for the three-body collision Rb + Rb + Yb^+. In this panel, the blue and red vertical dashed lines indicate the dissociation energies of $RbYb^+$ and Rb_2, respectively.

in the regime associated with $\beta = -4$, although for a small C_4 value (in the lower left part of the diagram in Fig. 2). The He_2 potential given in Table II is taken from Ref. 56, with dissociation energy $D_e \approx 10.48$ K, and the He_2^+ potential with $D_e \approx 2.85 \times 10^4$ K is from Ref. 58. The energy-dependent three-body recombination rate is calculated for collision energies between 1 mK and 10^4 K and is displayed in Fig. 9.

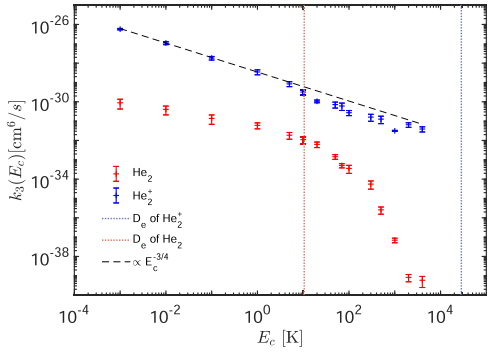

FIG. 9. Same as Fig. 7, but for He + He + He^+ three-body recombination. The blue and red vertical dashed lines indicate the dissociation energies of He_2^+ and He_2, respectively.

Unlike previous systems, in this case, the D_e of the molecule (He_2) is smaller than the D_e of the molecular ion (He_2^+). We notice an abrupt drop in the He_2 formation rate for collision energies larger than the dissociation energy of the molecule. On the contrary, the molecular ion formation rate follows the prescribed $E_c^{-3/4}$ (black dashed line) threshold law. However, we notice some deviations for collision energies larger than the dissociation energy of the molecule. This effect is so intriguing that it will be the subject of future work.

Finally, based on our results, it is confirmed that the formation rate of molecular ions in the low-energy regime is dominated by the long-range tail of the potentials and shows the same trend ($\propto E_c^{-3/4}$ with $\beta = -4$), independent of the A and B^+ species under consideration. However, this is not true for the reactions with collision energies beyond this regime, and, hence, it is necessary to consider both reactions—A + A + $B^+ \rightarrow$ A + AB^+ and A + A + $B^+ \rightarrow A_2 + B^+$—In particular, from the He + He + He^+ system, we conclude that the dissociation energy of AB^+ marks the limit of the low-energy regime, thus explaining why the threshold law is still fulfilled in the case of noble gas ions in their parent gases at 300 K.[10,43]

VI. CONCLUSIONS AND PROSPECTS

This work presents a study on ion–atom–atom three-body recombination using classical trajectory calculations in hyperspherical coordinates for collision energies ranging from 100 μK to 10^5 K. First, we have studied the parameter space extensively for long-range atom–atom and ion–atom potential combinations to find the behavior of the three-body long-range potential characterized by the β parameter. β can take any value between −4 (atom–ion dominated) and −6 (atom–atom dominated). As a result, it is possible to find three-body long-range potentials that depend on the interparticle distance different from the underlying pairwise interaction potential ($\beta = -5$). Moreover, the value of β relates to the production of molecules as against molecular ions. In particular, for $\beta = -4$, the production of molecular ions governs the reaction dynamics. In contrast, for $\beta = -5$ and $\beta = -6$, we find a comparable molecular formation rate between molecules and molecular ions and larger molecular formation than molecular ions in a wide range of impact parameters, respectively.

Next, we have studied four distinct ion–atom–atom systems, namely, Cs + Cs + Sr^+, Rb + Rb + Sr^+, Rb + Rb + Yb^+, and He + He + He^+. Considering our results, we conclude the following:

- Every charged–neutral–neutral, A + A + B^+, three-body recombination reaction shows a low and a high energy regime.
- The low collision energy regime is described by the β parameter, which characterizes the three-body long-range tail of the potential.
- The three-body recombination rate in the high-energy regime, as a function of the collision energy, shows a steeper trend compared to that in the low-energy regime. This behavior is due to the role of short-range atom–atom and atom–ion potentials in the reaction dynamics. As a result, we observe that the reaction rates for the production of molecular ions and neutral molecules are of the same order of magnitud—in stark contrast with the low-energy regime.
- The low- and high- energy regimes meet at collision energies comparable to the dissociation energy of the molecular ion.

In other words, the dissociation energy of the main reaction product establishes the transition energy between the low- and the high-energy regimes.

It is worth mentioning that in He + He + He^+ three-body recombination, we notice deviations from the predicted general trend of He_2^+ formation. This can be explained by noting the abrupt decrease of the formed He_2, due to its low dissociation energy (in contrast with the other three systems). Such an effect is so exciting and relevant that a more detailed study of this system will be published elsewhere.

Our results refer to the probability that a given product appears as a consequence of a three-body recombination reaction. Moreover, once a neutral molecule or molecular ion appears, it can undergo dissociation or quenching processes via interactions with other particles. These effects must be included for a proper simulation of the reaction dynamics. On the other hand, at very high collision energies, many-body effects in the ion–atom–atom potential energy surface may be relevant—a topic we plan to work on shortly. Finally, our findings reveal a universal trend in ion–atom–atom three-body recombination relevant to many fields: cold chemistry, chemical physics, astrochemistry, and plasma physics.

ACKNOWLEDGMENTS

The authors acknowledge the support of the Deutsche Forschungsgemeinschaft (DFG – German Research Foundation) under Grant No. PE 3477/2-493725479. J.P.-R. acknowledges the support of the Simons Foundation.

AUTHOR DECLARATIONS

Conflict of Interest

The authors have no conflicts to disclose.

Author Contributions

Marjan Mirahmadi: Formal analysis (equal); Investigation (equal); Methodology (equal); Writing – original draft (equal); Writing – review & editing (equal). **Jesús Pérez-Ríos**: Conceptualization (lead); Formal analysis (equal); Funding acquisition (supporting); Investigation (equal); Methodology (equal); Supervision (supporting); Writing – original draft (equal); Writing – review & editing (equal).

DATA AVAILABILITY

The data that support the findings of this study are available from the corresponding author upon reasonable request.

REFERENCES

[1] B. D. Esry, C. H. Greene, and J. P. Burke, Phys. Rev. Lett. **83**, 1751 (1999).
[2] J. Weiner, V. S. Bagnato, S. Zilio, and P. S. Julienne, Rev. Mod. Phys. **71**, 1 (1999).
[3] P. F. Bedaque, E. Braaten, and H.-W. Hammer, Phys. Rev. Lett. **85**, 908 (2000).
[4] H. Suno, B. D. Esry, and C. H. Greene, New J. Phys. **5**, 53 (2003).
[5] T. Weber, J. Herbig, M. Mark, H.-C. Nägerl, and R. Grimm, Phys. Rev. Lett. **91**, 123201 (2003).
[6] M. Schmidt, H.-W. Hammer, and L. Platter, Phys. Rev. A **101**, 062702 (2020).
[7] C. H. Greene, P. Giannakeas, and J. Pérez-Ríos, Rev. Mod. Phys. **89**, 035006 (2017).
[8] T. Köhler, K. Góral, and P. S. Julienne, Rev. Mod. Phys. **78**, 1311 (2006).
[9] D. Blume, Rep. Prog. Phys. **75**, 046401 (2012).
[10] J. Pérez-Ríos and C. H. Greene, J. Chem. Phys. **143**, 041105 (2015).
[11] A. Krükow, A. Mohammadi, A. Härter, J. H. Denschlag, J. Pérez-Ríos, and C. H. Greene, Phys. Rev. Lett. **116**, 193201 (2016).
[12] A. Mohammadi, A. Krükow, A. Mahdian, M. Deiß, J. Pérez-Ríos, H. da Silva, M. Raoult, O. Dulieu, and J. H. Denschlag, Phys. Rev. Res. **3**, 013196 (2021).
[13] N. Brahms, B. Newman, C. Johnson, T. Greytak, D. Kleppner, and J. Doyle, Phys. Rev. Lett. **101**, 103002 (2008).
[14] H. Suno and B. D. Esry, Phys. Rev. A **80**, 062702 (2009).
[15] N. Brahms, T. V. Tscherbul, P. Zhang, J. Kłos, H. R. Sadeghpour, A. Dalgarno, J. M. Doyle, and T. G. Walker, Phys. Rev. Lett. **105**, 033001 (2010).
[16] N. Brahms, T. V. Tscherbul, P. Zhang, J. Kłos, R. C. Forrey, Y. S. Au, H. R. Sadeghpour, A. Dalgarno, J. M. Doyle, and T. G. Walker, Phys. Chem. Chem. Phys. **13**, 19125 (2011).
[17] Y. Wang, J. P. D'Incao, and B. D. Esry, Phys. Rev. A **83**, 032703 (2011).
[18] N. Tariq, N. A. Taisan, V. Singh, and J. D. Weinstein, Phys. Rev. Lett. **110**, 153201 (2013).
[19] N. Quiros, N. Tariq, T. V. Tscherbul, J. Kłos, and J. D. Weinstein, Phys. Rev. Lett. **118**, 213401 (2017).
[20] M. Mirahmadi and J. Pérez-Ríos, J. Chem. Phys. **154**, 034305 (2021).
[21] M. Mirahmadi and J. Pérez-Ríos, J. Chem. Phys. **155**, 094306 (2021).
[22] J. Pérez-Ríos, Mol. Phys. **119**, e1881637 (2021).
[23] J. Pérez-Ríos, *An Introduction to Cold and Ultracold Chemistry* (Springer International Publishing, 2020).
[24] P. S. Krsti, R. K. Janev, and D. R. Schultz, J. Phys. B: At., Mol. Opt. Phys. **36**, L249 (2003).
[25] M. T. Cretu, M. Mirahmadi, and J. Pérez-Ríos, Phys. Rev. A **106**, 023316 (2022).
[26] R. S. Fletcher, X. L. Zhang, and S. L. Rolston, Phys. Rev. Lett. **99**, 145001 (2007).
[27] F. Palla, E. E. Salpeter, and S. W. Stahler, Astrophys. J. **271**, 632 (1983).
[28] D. R. Flower and G. J. Harris, Mon. Not. R. Astron. Soc. **377**, 705 (2007).
[29] M. J. Turk, P. Clark, S. C. O. Glover, T. H. Greif, T. Abel, R. Klessen, and V. Bromm, Astrophys. J. **726**, 55 (2011).
[30] R. C. Forrey, Astrophys. J. Lett. **773**, L25 (2013).
[31] D. Charlo and D. C. Clary, J. Chem. Phys. **120**, 2700 (2004).
[32] K. Luther, K. Oum, and J. Troe, Phys. Chem. Chem. Phys. **7**, 2764 (2005).
[33] M. Kaufmann, S. Gil-López, M. López-Puertas, B. Funke, M. García-Comas, N. Glatthor, U. Grabowski, M. Höpfner, G. P. Stiller, T. von Clarmann, M. E. Koukouli, L. Hoffmann, and M. Riese, J. Atmos. Sol.-Terr. Phys. **68**, 202 (2006).
[34] M. Mirahmadi, J. Pérez-Ríos, O. Egorov, V. Tyuterev, and V. Kokoouline, Phys. Rev. Lett. **128**, 108501 (2022).
[35] P. Weckesser, F. Thielemann, D. Wiater, A. Wojciechowska, L. Karpa, K. Jachymski, M. Tomza, T. Walker, and T. Schaetz, Nature **600**, 429 (2021).
[36] A. Krükow, A. Mohammadi, A. Härter, and J. Hecker Denschlag, Phys. Rev. A **94**, 030701 (2016).
[37] A. Härter, A. Krükow, A. Brunner, W. Schnitzler, S. Schmid, and J. H. Denschlag, Phys. Rev. Lett. **109**, 123201 (2012).
[38] H. Hirzler, E. Trimby, R. S. Lous, G. C. Groenenboom, R. Gerritsma, and J. Pérez-Ríos, Phys. Rev. Res. **2**, 033232 (2020).
[39] J. D. C. Jones, D. G. Lister, D. P. Wareing, and N. D. Twiddy, J. Phys. B: At. Mol. Phys. **13**, 3247 (1980).
[40] P. N. B. Neves, C. A. N. Conde, and L. M. N. Távora, Nucl. Instrum. Methods Phys. Res., Sect. A **580**, 66 (2007).
[41] P. N. B. Neves, C. A. N. Conde, and L. M. N. Távora, Nucl. Instrum. Methods Phys. Res., Sect. A **619**, 75 (2010).
[42] V. O. Papanyan, G. T. Nersisyan, S. A. Ter-Avetisyan, and F. K. Tittel, J. Phys. B: At., Mol. Opt. Phys. **28**, 807 (1995).
[43] J. Pérez-Ríos and C. H. Greene, Phys. Rev. A **98**, 062707 (2018).
[44] H. Pollard, *Celestial Mechanics* (American Mathematical Society, 1976).
[45] Y. Suzuki, Y. Varga, M. Suzuki, and K. Varga, *Stochastic Variational Approach to Quantum-Mechanical Few-Body Problems* (Springer, 1998).
[46] C. D. Lin, Phys. Rep. **257**, 1 (1995).

[47]J. Avery, *Hyperspherical Harmonics: Applications in Quantum Theory*, Reidel Texts in the Mathematical Sciences (Springer Netherlands, 2012).
[48]J. Pérez-Ríos, S. Ragole, J. Wang, and C. H. Greene, J. Chem. Phys. **140**, 044307 (2014).
[49]L. F. Shampine and M. W. Reichelt, SIAM J. Sci. Comput. **18**, 1 (1997).
[50]Y. Wang, M. Mirahmadi, A. A. Elkamshishy, and J. Pérez-Ríos, Few-Body Syst. **64**, 6 (2023).
[51]W. Weickenmeier, U. Diemer, M. Wahl, M. Raab, W. Demtröder, and W. Müller, J. Chem. Phys. **82**, 5354 (1985).
[52]M. Aymar, R. Guérout, and O. Dulieu, J. Chem. Phys. **135**, 064305 (2011).
[53]P. Schwerdtfeger and J. K. Nagle, Mol. Phys. **117**, 1200 (2019).
[54]C. Strauss, T. Takekoshi, F. Lang, K. Winkler, R. Grimm, J. Hecker Denschlag, and E. Tiemann, Phys. Rev. A **82**, 052514 (2010).
[55]E. R. Sayfutyarova, A. A. Buchachenko, S. A. Yakovleva, and A. K. Belyaev, Phys. Rev. A **87**, 052717 (2013).
[56]R. A. Aziz, A. R. Janzen, and M. R. Moldover, Phys. Rev. Lett. **74**, 1586 (1995).
[57]H. M. Hulburt and J. O. Hirschfelder, J. Chem. Phys. **9**, 61 (1941).
[58]D. T. Chang and G. I. Gellene, J. Chem. Phys. **119**, 4694 (2003).